This is an author-formatted pre-final version of the paper published in IEEE/ASME Transactions on Mechatronics, vol. 26, no. 5, 2021 (winner of the 2021 IEEE/ASME Transactions on Mechatronics Best Paper Award).
See https://doi.org/10.1109/TMECH.2020.3043454 for the final published version.

Blindly Controlled Magnetically Actuated Capsule for Noninvasive Sampling of the Gastrointestinal Microbiome

Peyman Shokrollahi, Yung P. Lai, Samrand Rash-Ahmadi, Victoria Stewart, Mohsen Mohammadigheisar, Lee-Anne Huber, John Parkinson, and Eric Diller

***Abstract*— *Objective:* To address the challenges of physical sample retrieval from all locations along patients' gastrointestinal (GI) tracts for studying of interactions between GI microbial communities (microbiomes) and host immune systems. *Methods:* We propose a novel tetherless magnetically-actuated capsule for noninvasive sampling of GI microbiomes and liquid digesta. The mesoscale capsule, a soft mobile robot platform, is made from two permanent magnets encapsulated in a soft elastomer and actuated remotely by an external magnet. Following oral administration, capsules transit the GI tract and are activated at specified locations. Samples are recovered via routine stool passage and processed for downstream analyses (e.g. 16S rRNA surveys, metagenomics, metatranscriptomics and/or metabolomics). A mathematical model is derived to predict capsule activation and guide design optimization. *Results:* We demonstrate both the ability of the capsule to collect samples, as well as maintain sample integrity *in vitro* and *in vitro*, and with twelve capsules in *in vivo* swine models. Eleven capsules successfully collected digesta (in the range of 18 to 61 mg). Conclusion*:* The capsule successfully collected and sealed samples. *Significance:* This sampling apparatus offers a technological advance for the robust sampling of GI tract contents.**

***Index Terms*— Magnetic Actuation, Microbiome, Microrobotics, Noninvasive Sampling, Soft robotics.**

I. Introduction

The mammalian gut is home to a complex community of microbes, termed the microbiome. Increasingly, the composition and function of the gut microbiome in humans has been linked to a large range of diseases including diabetes and inflammatory bowel disease (IBD) [1-5]. From a livestock perspective, global bans on the use of dietary supplementation of antibiotics is driving interest in the identification of alternative strategies, such as probiotic feed additives, for promoting growth through the manipulation of the gut microbiome. The key to developing new therapeutic strategies in the case of human disease, or novel feed additives in the case of livestock production, is an improved understanding of the interactions between the gut microbiome and the host immune system. A major challenge to such an understanding is the retrieval of physical samples that inform on the composition and function of the microbiome from physiologically-relevant sites within the GI tract. While the composition and activity of microbes vary dramatically across the GI tract [6], [7], studies of the gut microbiome typically rely on the use of stool samples that are not reflective of intestinal sites relevant to disease or nutrient absorption.

One approach to obtain more informative samples is the use of endoscopy. However, endoscopy is highly invasive, expensive, and in humans typically used only for initial diagnosis. In addition, distal regions of the small intestine are not accessible without the use of invasive instrumentation and procedures. Consequently, there has been much interest in developing less invasive devices capable of sampling from internal regions on a more regular basis [8]-[11]. For example, Kerkhof proposed a device to sample liquids [12], but because it uses pH-sensitive material to control sampling timing, the device may operationally fail due to the dependency on the pH level. Jones et al. [13] recently proposed other ingestible designs for GI tract microbiome sampling, but that actuator system is complex, with a multistage valve system, which increases the risk of failure and limits the potential for scaling to smaller size of capsule. Cui et al. [14] developed a micromachined capsule which has a relatively large size compared to the confined GI tract space, and thus has a risk of retention in the body, similar to endoscopic capsules [15], [16].

As a magnetic field can penetrate biological materials into the body, it is suitable for the remote control of a capsule in

This research was supported by the Medicine by Design New Ideas Fund MbDNI-2017-02.

P. Shokrollahi, Y. Lai and E. Diller are with the Department of Mechanical and Industrial Engineering, University of Toronto, Toronto, ON M5S3G8 Canada (e-mail: peyman.shokrollahi@utoronto.ca, yp.lai@mail.utoronto.ca, eric.diller@mail.utoronto.ca).

S. Rash-Ahmadi is with the Department of Mechanical Engineering, Urmia University, Urmia, Iran (e-mail: s.rashahmadi@urmia.ac.ir).

L. Huber, V. Stewart and M. Mohammadigheisar are with the Department of Animal Biosciences, University of Guelph, Guelph, ON, N1G2W1, Canada (email: huberl@uoguelph.ca, vstewa01@uoguelph.ca, mmohamm@uoguelph.ca).

J. Parkinson is with the Department of Biochemistry & Molecular and Medical Genetics, University of Toronto, Toronto, ON M5S1A8 Canada (e-mail: john.parkinson@utoronto.ca).

inaccessible regions such as the small intestine [17]. A magnetic actuation mechanism does not require onboard control and power circuits, permitting device size downscaling and the allocation of more space for sample collection volume [18]. Magnetic fields have been used to apply force and torque to control a variety of medical devices inside the body [19]. Several groups have developed active robotic capsule endoscopes [19], focusing on the development of magnetically actuated controllable endoscopes [20]–[23] and enhanced capsules for drug delivery [24]–[26]. These capsules cannot be used for microbiome or digesta sampling and no stand-alone small-scale completely soft robot for microbiome sampling across all locations in the GI tract has been developed.

We thus propose a novel tetherless magnetically actuated capsule (MAC) for noninvasive sampling of liquid digesta containing GI microbiomes. Constructed as a capsule of outer diameter 8 mm and length 11, the MAC is a soft mobile robot platform comprised of two permanent magnets encapsulated in a soft elastomer with hinge and sampling container. Following oral administration, the capsule transits the GI tract passively and is activated remotely for sampling by an external magnetic field. A patient could swallow multiple capsules (at various time points), which could be activated at once. The capsules are recovered via routine stool passage. Microbiome samples are encapsulated and sealed in the device during passage through the GI tract and processed upon retrieval for downstream analysis of microbiome composition and/or function (e.g. 16S rRNA surveys, metagenomics, metatranscriptomics and/or metabolomics). In this paper we introduce the design and activation mechanism of the robotic capsule, show its reliable operation under application conditions, and report on *in vitro* and *in vivo* experiments proving the sampling capability.

For safe and successful activation, the capsule must incorporate two desired features: blind robust activation and a soft body. Additional design requirements must be met in activation, sealing, compatibility, and material strength:

A. Blind Activation

Activation means opening the capsule chamber wide enough using an external magnetic field to collect a liquid microbiome sample blindly (i.e., when the capsule has an unknown location and orientation) into the capsule reservoir. Blind activation will be tested by activating the capsule inside the animal's GI tract without using any localization system. Given the size of the target swine, activation must be accomplished at distances within the body of up to 15 cm. In addition, the collected sample volume should be as large as possible to fill the sampling reservoir.

B. Sealing

Sealing means keeping the capsule closed before and after activation, preventing digesta leakage into and out of it, thereby preventing cross-contamination of collected samples with other liquids during capsule transition through the GI tract under conditions such as agitation and irregular motion. Sealing will be tested by agitative motions applied to the capsule.

C. Material Strength

Material strength should be sufficient for the capsule to tolerate various external and internal forces and torques during ingestion, GI transit and collection after passage in the feces. The material should not collapse under the attraction force used for sealing. It should be strong enough that the capsule opens and closes safely, without damage to its parts, especially the hinge site. Strength will be tested by performing tensile and capsule agitation tests as well as in-vivo experiments in swine.

D. Compatibility

Compatibility means that the materials coming into contact with tissue are safe, acid- and enzyme-resistant, and do not inhibit cell viability of collected samples. The capsule materials must remain intact while operating in the low-pH environment of the GI-tract with various enzymatic activity. Compatibility will be tested by performing a cell viability test.

II. Design and Operation

To achieve the above specifications, the MAC was designed and implemented as follows.

A. Structural Design and Activation Mechanism

To address the engineering challenge of blind tetherless activation for noninvasive procedures, the MAC is designed as a compliant, small (8-mm outer diameter, 11-mm length), cylindrical silicone rubber composite capsule as shown in Fig. 1. Each of its two sides contains a disk magnet (type N52; 0.6 cm diameter, 0.3 cm thickness; magnetization direction along the diameter) and a cylindrical chamber (28.9–38.5 μL volume) for sample storage during GI tract transit. The two sides of the capsule are connected by a hinge. The entire capsule besides the internal magnets is soft, composed of a composite developed to ensure that 1) the capsule does not collapse under deformation, 2) the magnets are held securely in place, and 3) the body and hinge site are reinforced. The capsule is closed until it is opened via application of an external magnetic field (Fig. 1). This applied magnetic field generates a torque on each internal magnet to bring it into alignment with the field. The effect of the applied field is thus to create an opposite magnetic torque on each capsule magnet, which opens the capsule. The opposite directions of the two internal magnets also generate an inter-magnet attraction force to seal the capsule. This attraction force is an important part of the design; its precise magnitude satisfies the capsule sealing property for safe sample transit while still allowing capsule opening with minimal external magnetic field application.

The external magnetic field must be applied in the correct direction to open the MAC. Thus, the capsule is designed with a small net magnetic moment to allow the entire capsule body to self-align with the applied field into the correct heading. This slight magnetic moment is created by introducing a small angle α_0 to the internal magnets as shown in Fig. 2.

The MAC magnetic opening operation mechanism is illustrated in Fig. 2, where an applied field $\boldsymbol{B}_{ext}$ will create opposing magnetic torques $\boldsymbol{T}_{ext}$ on each of the opposing magnets. This torque balances with the hinge torque $\boldsymbol{T}_h$ and the

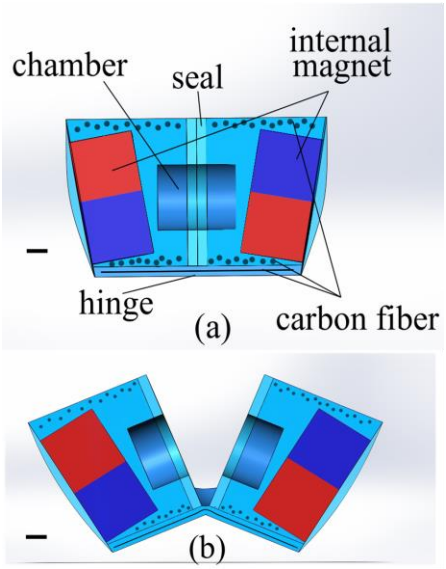

Fig. 1. The magnetically actuated capsule, closed (a) and opened (b). Each of the two symmetrical sides has a chamber, internal magnet, carbon fiber, and sealing mechanism. (scale bar, 1 mm).

interaction force and torque between the two magnets $\boldsymbol{F}_1$ and $\boldsymbol{T}_1$.

When multiple capsules are used together, the ingestion intervals should be designed to avoid the capsules clumping in the stomach as they will attract each other magnetically. The median gastric transit time (time to pass the stomach) for endoscopic capsules is 21 min in the literature [27]. Capsules should thus be fed no sooner than approximately 45 minutes from each other. Typical GI-tract transit times in humans, as studied for drug delivery systems, are 3 and 24 h for the small and large intestines, respectively [24].

One large external permanent magnet, or several stacked or parallel magnets [29][30], are used to activate the capsule, depending on the patient/animal size. The magnet(s) of approximately 1.5 kg are manually handled and inexpensive as compared with electromagnets, enabling a flexible approach, but with risks of low precision and failure due to manual capsule activation. In this work we activate the capsule blindly by moving the external permanent magnet over the body, thus exposing the entire body to the magnetic field over the duration of activation.

Regarding capture enhancement, the volume of sample collected depends in part on the affinity of the digesta to the inner surface of the capsule chamber. The surface energy of this inner cavity was increased to maximize this affinity and increase the collected sample size. Given its ease of use, biocompatibility, and previous use to improve cell adhesion to silicone rubber surfaces [28], polydopamine was used as a hydrophilic coating on the rubber.

B. Sealing Mechanism Development

To fulfill the requirements of the sealing specifications, silicone rubber was used with enough adhesion force to avoid leakage and sample contamination. A silicone rubber more compliant than that used in the MAC structure was used to create a seal between the capsule sides. This lower stiffness

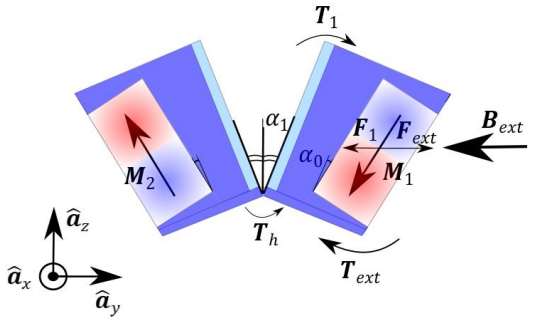

Fig. 2. Two internal permanent disk magnets show at a slanted at angle α_0, resulting in net magnetization (to the left here) when the capsule is closed. Applied magnetic torques and inter-magnet forces are shown on the right-half of the MAC as a free-body diagram.

rubber was created by using approximately 40% less curing catalyst, which in turn reduced the amount of crosslinking and resulted in less stiffness.

C. Composite Development

To address the challenges of material strength, a silicone rubber carbon fiber composite is used to reinforce the capsule body and hinge, providing sufficient strength for the hinge to tolerate the force and torque applied for capsule opening. The hinge also contributes to capsule closure when the external field is removed. The composite was developed to provide sufficient strength such that the capsule does not open too far – beyond a certain pivot point the internal magnets stick together in the fully 'folded-back' open configuration. The composite hinge also prevents the capsule halves from breaking apart on application of a strong external field.

The hinge is the most vulnerable part of the MAC design; it must not break upon capsule activation. As the capsule is activated blindly at an unknown distance from the external magnet, a large external field is generally required to ensure the MAC is opened. With a stiff hinge, a low field could not open the capsule. However, the hinge should be able to tolerate the force applied when the capsule is close to superficial body surfaces and the field is large.

D. Compatibility

To validate the silicone rubber compatibility, the alamarBlue (Thermo Fisher) viability test that is a standard for quantifying cell viability was performed based on the protocol provided in [31]. Silicone rubber samples were incubated with fibroblast media for 1, 3, and 7 days. Fibroblast cells (3×10^4 cells/well) were seeded in a 96-well plate and fed with incubated media (500 µL) for 1 day, followed by comparison with unincubated samples. To evaluate cell viability, 50 µL alamarBlue was added to each well. After 4 h incubation at 37°C in a humidified atmosphere of 5% CO_2 and 95% air, fluorescence was measured with a cyto-fluorometer adapted to a microplate (λ_{ex}: 555 nm, λ_{em}: 585 nm) using a SpectraMax i3 multimode microplate reader (Molecular Devices).

III. Analytical Model

Capsule functionality requires control of the forces and

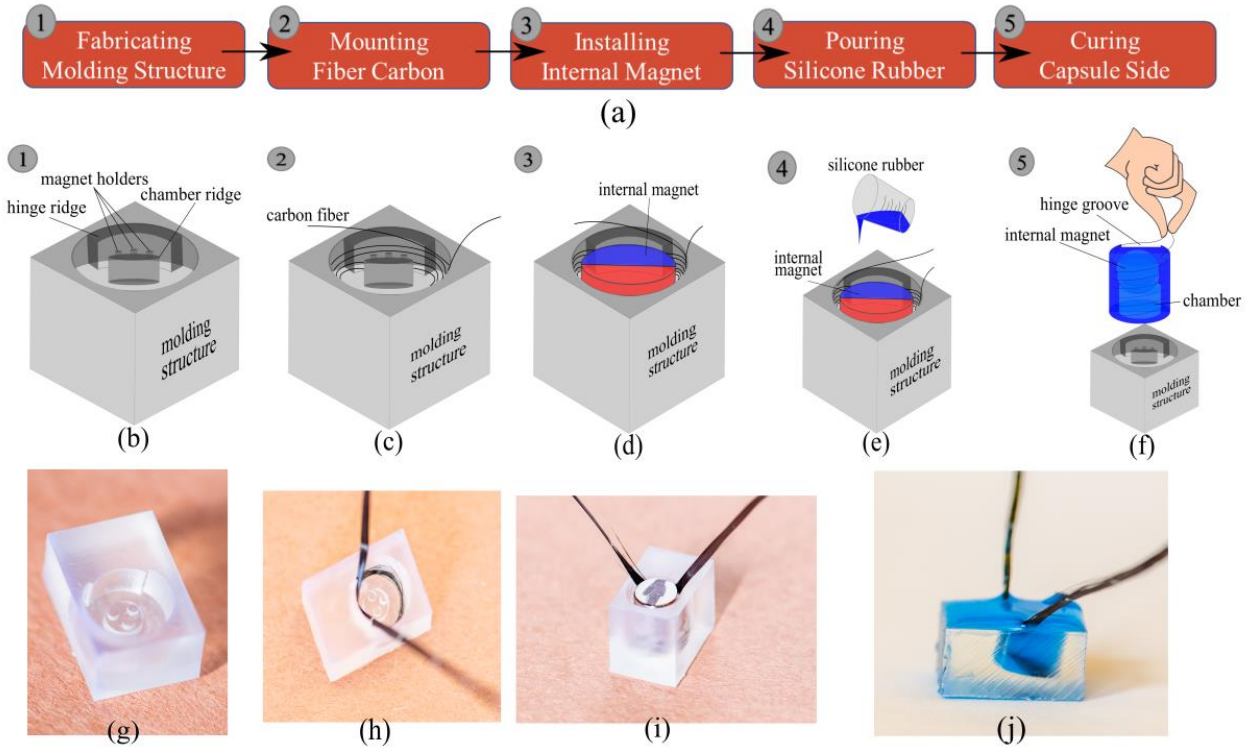

Fig. 4. (a) MAC fabrication steps for the two capsule halves. (b, g) The capsule end molding structure (c, h) carbon fiber mounting within the mold, (d, i) internal magnet installation, (e) pouring of silicone rubber, and (f, j) curing of the capsule sides.

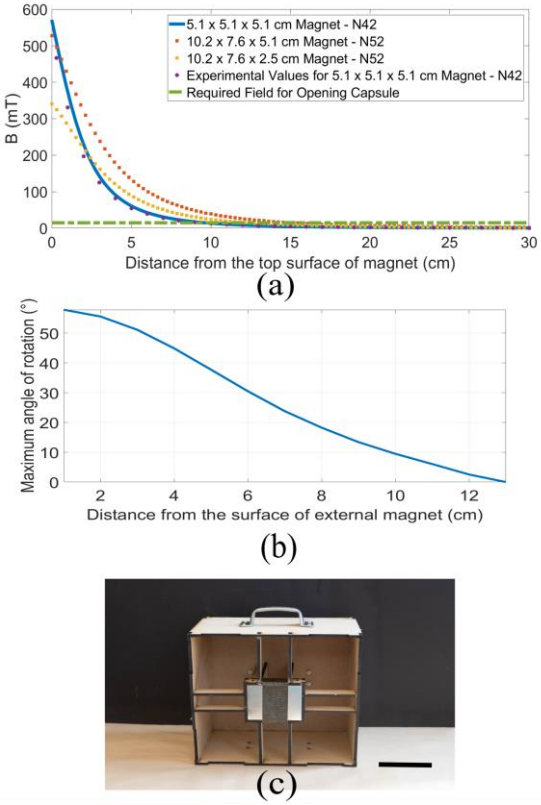

Fig 3. (a) Calculated B-fields for three rectangular magnets using a charge model, compared with one experimental measurement. The field required to open the capsule is 15 mT. (b) Maximum allowable angular misalignment of the external magnet which still results in the field strength meeting the 15 mT minimum activation threshold. (c) Magnet safety box for external capsule activation, showing the magnet in the centre surrounded by open space. Scale bar, 10 cm.

torques involved in its opening and closing. An analytical model of capsule opening is used to inform the overall design of the MAC system, including the selection and placement of internal and external magnets for proper sealing and blind opening as well as geometric design of the capsule hinge.

A. Model for the Internal Magnets

The magnetic opening torque scales with the volume of the internal magnets. Thus, the largest internal magnet volume (considering GI tract limitations) and highest grade were selected to generate a strong internal magnetic moment.

The internal magnets can be approximated by a dipole magnetic moment of $\boldsymbol{m}_1$ for the right side and $\boldsymbol{m}_2$ for the left side. This magnetic moment is a vector pointing from the south to north magnetic pole of the internal magnet proportional to the magnet strength. Relevant magnetization vectors ($\boldsymbol{M}_1$ and $\boldsymbol{M}_1$) are labeled on the capsule free body diagram (Fig. 2), and $\boldsymbol{m}_1 = \boldsymbol{M}_1 V$ and $\boldsymbol{m}_2 = \boldsymbol{M}_2 V$, where V is the magnet volume, are equal for both internal magnets. Each internal magnet will experience a torque and force generated by the other internal magnet as well as an activating torque and force generated by the externally-applied magnetic field. The torque on an internal magnet $\boldsymbol{m}$ due to an applied field $\boldsymbol{B}$ is $\boldsymbol{m} \times \boldsymbol{B}$, which acts to bring the magnetic moment into alignment with the field. The magnetic force on an internal magnet is created by a field gradient and is $(\boldsymbol{m} \cdot \nabla)\boldsymbol{B}$, which acts approximately to move magnets towards regions of higher field strength.

The internal torque and force applied to $\boldsymbol{m}_1$ by the other magnet $\boldsymbol{m}_2$ are $\boldsymbol{T}_1$ and $\boldsymbol{F}_1$, respectively. The activating torque and force on $\boldsymbol{m}_1$ by the external field $\boldsymbol{B}_{ext}$ are $\boldsymbol{T}_{ext}$ and $\boldsymbol{F}_{ext}$, respectively. The hinge also generates a resistive torque for

capsule opening τ_h. These forces and torques on the capsule half 1 sum and are balanced at a certain capsule opening angle α according to the torque balance equation

$$\boldsymbol{T}_1 + \boldsymbol{L} \times \boldsymbol{F}_1 + \boldsymbol{\tau}_h + \boldsymbol{m}_1 \times \boldsymbol{B}_{ext} = 0 \quad (1)$$

where $\boldsymbol{L}$ is the position vector originating from the hinge center of mass (COM) to the internal magnet COM (Magnet 1). The total angle α is the sum of the small offset angle α_0 and half of opening angle α_1. To calculate the field and field gradient generated by the internal magnet for use in (1), a dipole field model is used.

$$\boldsymbol{T}_1 = -\frac{\mu_0 m^2}{8\pi r^3}\sin(2\alpha)\,\hat{\boldsymbol{a}}_x \text{ and} \quad (2)$$

$$\boldsymbol{F}_1 = \frac{3\mu_0 m^2}{4\pi r^4}\left(-1 - \sin^2(\alpha)\right)\hat{\boldsymbol{a}}_y, \quad (3)$$

where μ_0 is the magnetic permeability of free space (1.257×10^{-6} H/m), $m = m_1 = m_2$, r is the distance between the COMs of the internal magnets, and $\hat{\boldsymbol{a}}_x$ and $\hat{\boldsymbol{a}}_y$ are the unit vectors of the coordinate system indicated in Fig. 2.

Therefore, Equation 1 can be expressed as follows:

$$\frac{\mu_0 m^2}{8\pi r^3}\sin(2\alpha)\,\hat{\boldsymbol{a}}_x + \frac{3\mu_0 L m^2}{4\pi r^4}(1 + sin^2\alpha)\cos(\alpha' + \alpha_1)\,\hat{\boldsymbol{a}}_x + \left(\frac{3EI\tan(\alpha_1)}{l'}\right)\hat{\boldsymbol{a}}_x - mB_{ext}\cos(\alpha)\,\hat{\boldsymbol{a}}_x = 0, \quad (4)$$

where r is the distance between the COMs of the internal magnets, and α' is the angle between the plane intersecting both halves of the capsule and the plane passing through the COMs of the hinge and internal magnet across the capsule diagonally. The hinge torque ($\boldsymbol{\tau}_h$) is approximated with the elastic model of a rectangular cantilever beam using the Euler–Bernoulli theory, where l' is the length of the hinge, E is the Young's modulus calculated experimentally from the results of the tensile test, and I is the second moment of area. The hinge geometrical properties (e.g., thickness and length) play critical roles in Equation 4.

The internal permanent magnets (type N52; 0.6 cm diameter, 0.3 cm thickness; K&J Magnetics Inc.) are magnetized in the direction of their diameter and are mounted in the capsule.

The magnitude of magnetic moment was determined as approximately 0.124 Am^2. This value was evaluated by measuring the magnetic field versus distance and fitting a dipole model to approximate the magnitude of the magnetic moment. This value is very close to reported one by the manufacturer as 0.1178 Am^2.

The key design consideration contributing to the control of capsule opening and closing in this model is the placement of the magnet within each half of the body, parameterized by the position vector $\boldsymbol{L}$. Our capsule design was generated through a trial and error process by choosing $\boldsymbol{L}$ which results in sufficient sealing force but also the ability to open the capsule under the available magnetic field from the external magnet. The MAC opening angle will later be calculated and experimentally characterized as a function of the applied external field (see Fig. 6).

B. Model for the External Magnet

Due to sealing adhesion, inter-magnet attraction within the capsule as well as the hinge torque, the field required to open the capsule has some minimum threshold.

The $\boldsymbol{B}$ field generated by the external magnet is studied in Fig. 3a) for three different external magnet sizes which are commercially available and not too large to safely handle. Due to the large size of the external magnet and its relatively flat rectangular shape, a dipole field model does not accurately capture the magnetic field at near distances from magnet. Thus, a charge model is used. In this model, the permanent magnet is modeled with a distribution of volume (ρ_m) and surface (σ_m) magnetic charges. The volume and surface charge densities are calculated as $\rho_m = -\nabla.\boldsymbol{M}$ and $\sigma_m = \boldsymbol{M}.\hat{\boldsymbol{n}}$, respectively, where $\boldsymbol{M}$ is a magnetization vector and $\hat{\boldsymbol{n}}$ is a surface normal vector. Due to uniform polarization, $\boldsymbol{M} = M_S\hat{\boldsymbol{a}}_z$, thus $\rho_m = -\nabla.\boldsymbol{M} = 0$ and the model is simplified to a surface charge distribution [32]. The $\boldsymbol{B}$ field along the central axis (z) of the magnet is calculated as [32]:

$$B(z) = \frac{\mu_0 M_S}{\pi}\left[tan^{-1}\left(\frac{(z+L)\sqrt{a^2+b^2+(z+L)^2}}{ab}\right) - tan^{-1}\left(\frac{z\sqrt{a^2+b^2+z^2}}{ab}\right)\right], \quad (5)$$

where a and b are the dimensions of the front surface and L is the thickness of a magnet bar. In Fig. 3a, the $\boldsymbol{B}$ field is plotted as a function of the distance (z) from the front surface.

Because the external magnet is manually controlled by hand, we also studied the effect of small angular misalignments of the external magnet from the capsule true location. A properly aligned external magnet points the external magnet directly at the capsule. However, during blind activation of the capsule, the external magnet will be scanned systematically over the entire abdomen but will likely not point directly at the capsule when at its closest approach point. This effect is shown in Fig. 3b, where the maximum angle error from nominal is plotted as a function of the external magnet misalignment. Below this maximum angle threshold, the field will still be above the minimum required 15 mT to open the capsule.

From these results, we chose the intermediate-size external magnet (type N52, 10.2 × 7.6 × 2.5 cm; K&J Magnetics Inc., magnetized along its thickness) because it is easier to handle than the largest type, and still generates a large enough field for capsule activation. The external magnet is secured within a magnet safety box (Fig. 3c) for safe handling during swine testing.

IV. Fabrication

In this section we describe the fabrication of the sampling capsule according to the design parameters set out in Section II. In three steps, the separate capsule sides, sealing mechanism, and hinge are fabricated. The three pieces are then assembled.

A. Capsule Side Fabrication

A molding structure consisting of a hinge ridge, chamber ridge (creating cavities for the respective components), and magnet holders was created as outlined in Fig. 4. A unidirectional carbon fabric (2585-A; Fibre Glast Developments Corp.) was wrapped around the chamber. Magnets were mounted on the holders, designed to orient the magnets at small offset angle α_0, in the mold. Here α_0 was chosen as 10° which is a compromise between capsule

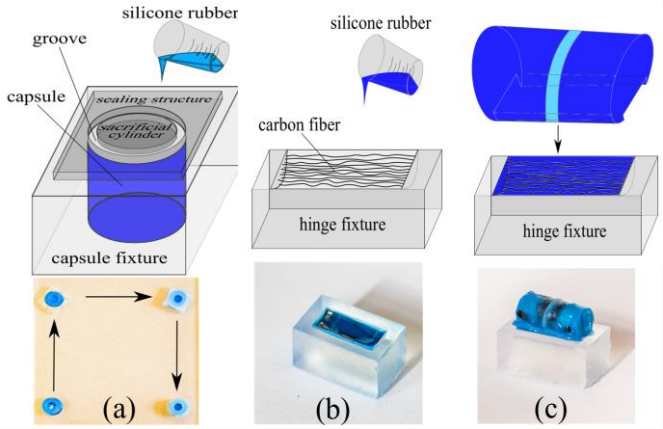

Fig. 5. (a) The four-stage process of sealing mechanism preparation, (b) mounting of carbon fiber in the hinge fixture and pouring of silicone rubber, and (c) mounting of the capsule in the hinge structure and curing of the hinge.

activation strength and net magnetic moment strength for capsule orientation control. During curing, the internal capsule magnets were held in the correct orientation by a magnetic field used as a fixture, generated by 2.5 cm cubic magnets (type N52; K&J Magnetics Inc.). The external magnet and mold were mounted on a physical fixture to maintain magnet directionality.

Silicone rubber (Mold Star 30, Smooth-On Inc.) was used at a 1:1 mass ratio of A and B parts from the manufacturer. The rubber was degassed in a vacuum chamber before and after pouring into the mold. The capsule sides were left overnight to cure.

B. Sealing Mechanism Fabrication

On the chamber, three orifices caused by the attachment of the magnet to the magnet holders were repaired by injection of the same silicone rubber (Mold Star 30). Then, the prepared capsule sides were mounted on a fixture for seal fabrication (Fig. 5a). A sacrificial cylinder was inserted into the chamber to form the seal geometry precisely around the rim of the capsule halves. The sealing structure and sacrificial cylinder were cubic and cylindrical laser-cut acrylic sheets with dimensions of 10 mm and diameter of 4 mm, respectively.

Degassed Mold Star 30 (10:1 mass ratio of parts A to B) was poured into the groove between the sealing structure and sacrificial cylinder and cured for 12 h. Then, the cylinder and structure were removed from the capsule side for hinge preparation.

C. Hinge Mechanism Fabrication

For the MAC hinge, the composite was reinforced with carbon fibers (2585-A; Fibre Glast Developments Corp.). Before and after fiber mounting in the hinge fixture, Mold Star 30 (1:1 mass ratio of parts A to B) was poured into the fixture. Then, the attached capsule sides were mounted in the composite and the hinge was left overnight to cure (Fig. 5 b and c).

D. Internal Coating for Capture Enhancement

Dopamine hydrochloride (Sigma-Aldrich) was dissolved in Tris-HCl buffer (10 mM, pH 8.5 [adjusted by addition of 37% HCl]) to a concentration of 2 g/L to create the polydopamine solution as in [28]. The polydopamine solution was then placed into both sides of the capsule chamber (20 µL each) for 24 hours under air. The chambers were then flushed and washed three times with deionized water for 10 min with sonication and dried at room temperature overnight.

V. Experiments

A. In Vitro Experiments

An in-vitro experiment was performed to determine the required magnetic field and minimum capsule–external magnet (type N52, 10.2 × 7.6 × 2.5 cm) distance for activation. The magnet's magnetic field was measured five times at various external magnet-to-capsule distances to determine the field required for activation. This measurement was repeated for 12 different capsules. The average distance required for activation was 5.3 cm, with a 15-mT field required for activation (to overcome internal torques and the adhesion caused by the sealing surfaces of the two capsule halves).

To test capsule sealing, we performed a MAC agitation experiment. Here 10 µL of green food dye was injected into the sampling chambers of five capsules. Each was immersed individually in a 10-mL tube filled with 50 mL deionized water. The tubes were then agitated in a centrifuge (Sorvall Legend X1R; Thermo Scientific) at 300 rpm for 1 h at 25°C. Then, they were vortexed at maximum speed for 5 min in an analog vortex mixer (VWR International, LLC). To test how much green food dye escaped the capsule during this agitation, a calibration curve of five known dye concentrations (0.02, 0.01, 0.0075, 0.005, and 0 vol%) were made and the average concentration of food dye in the water of vortexed capsules was determined by UV-vis spectroscopy (Cary 50 UV-Vis spectrophotometer, Agilent Technologies). The seal was effective in preventing major leakages of dye out of the capsule (0.001 ± 0.0004 vol% dye in water after vortexing, $n = 5$).

Capsule self-alignment to an applied field was tested in an acrylic tub container. MAC orienting, activating, swiveling, summersaulting, and stopping actions were tested by moving the magnet around a beaker in which the capsule was immersed in water, with the resulting motion shown in Supplementary Video 1.

B. Opening Angle Determination

To experimentally measure the opening angle of the capsule under different external magnetic field strengths, we applied fields in a Helmholtz electromagnetic coil set. In this coil pair, precise coil currents are applied by three analog servo drives (30A8; Advanced Motion Controls). Custom control code was used with a multifunction analog/digital I/O board (model 826; Sensoray) to control the coil current. Coil calibration was performed with a gaussmeter (LakeShore Cryotronics). Two cameras (FO134TC; FOculus) at the coil side and top were used at 30 frames/second to provide a view of the capsule opening motion. The coil system can generate a uniform field up to 18 mT in arbitrary three-dimensional directions near its geometric center, with ± 5% error within a 44 mm sphere.

Each of five capsules was placed in the center of the coil. Top-view images were obtained in parallel projection (i.e., parallel to the lateral capsule view) for capsule opening angle measurement. Side-view images were used to indicate the capsule position to ensure the MAC was located in the center of

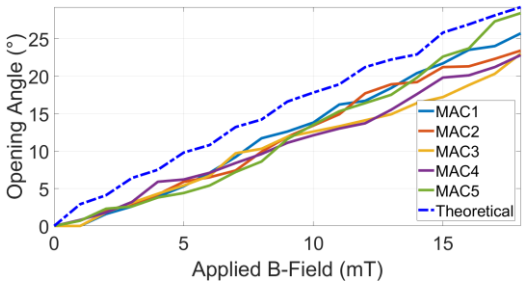

Fig. 6. Opening angle vs. applied field for five capsules in the coil. The dashed line indicates the theoretical results derived from solving of the torque equilibrium equation. The opening angle is $2\alpha_1$ (defined in Fig. 2).

the coil's workspace to ensure field uniformity. The magnetic field was applied along the capsule long axis. The capsules moved freely in contact with the bottom of the coil's working space, permitting symmetrical opening of both sides. To avoid surface tension and adhesion caused by the soft capsule seal during the opening time of the capsules, the magnetic field was first applied at 18 mT to fully open the capsule and then decreased to near zero. The opening angle as a function of applied field, reported in Fig. 6, was identified from recorded images using the open-source Tracker software [33].

C. Hydrophobicity Analysis

The capturing capability of the capsule during the activation is partially dependent on the hydrophobicity of the chamber site. To study this and assess the potential to improve the surface wetability, the contact angle of water and diiodomethane were measured on five uncoated silicone rubber samples and five coated silicone rubber samples (2 g/L dopamine in Tris-HCl buffer, 24 hours) three times each sample using a contact angle goniometer (OCA 15EC; Dataphysics). The water contact angles (mean ± SD, n = 15) were 104.5 ± 3.7° and 54.8 ± 6.0° for uncoated and coated silicone rubber, respectively. The surface energies (mean ± SD, n = 15), calculated as in [34], were 23.4 ± 1.4 and 44.5 ± 4.8 mN/m for uncoated and coated rubber, respectively. Polydopam decreased the water contact angle and doubled the surface energy, providing hydrophilic coating of the silicone.

D. Tensile Analysis

The silicone rubber by itself is not strong enough to hold the capsule closed during vigorous motion in the stomach of swine model. Therefore, we developed a composite reinforced with carbon fibers aligned longitudinally in the direction of the hinge as described in Section III. A tensile test was performed with two samples each of this composite and silicone rubber using an Instron 4465 universal tensile tester with a crosshead speed of 50 mm/min, based on International Standard ISO-527. The stress-strain curves showed that the maximum tensile strength (12 MPa) of the carbon fiber composite was six times greater than that of the pure rubber (2 MPa).

E. Acid Resistivity

The biological environment of the GI tract is not hostile to silicone rubber, except in the stomach which contains hydrochloric acid with low pH (< 4) [35][36]. As the capsule may stay in the stomach for up to several hours during gastric transit, its outer shell should be acid resistant by maintaining its

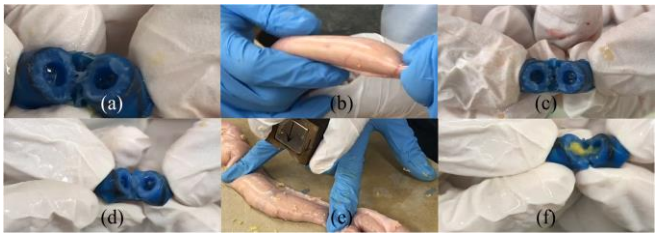

Fig. 7. (a) Inspecting capsule emptiness before insertion into the intestine section for the sealing test, (b) mechanical agitation of the intestine with the capsule inside, and (c) opening of the capsule after transit. (d) Inspecting capsule emptiness before insertion into the intestine for the activation test, e) capsule activation with a 5.1 cm cubic magnet, and f) inspection of digesta collection by one representative capsule.

elastic and strength properties. To test the potential for rubber damage in acid, ten dumbbell-shaped samples were prepared according to ASTM 412-416 standard (Die C) for vulcanized rubber and thermoplastic elastomers. Five samples were immersed in hydrochloric acid (pH 1.2) for 24 h. Afterwards, the tensile properties of the 10 samples were measured using an Instron 4465 universal tensile tester with a crosshead speed of 50 mm/min, based on International Standard ISO-527.

Stress-strain curves were analyzed, where a *t*-test of ultimate tensile strength yielded a p value of 0.22 between samples that were exposed and those unexposed to acid, indicating no significant difference in tensile strength between acid-treated and untreated samples. No significant difference in the tangent modulus was observed and scanning electron microscope images of the rubber surface showed no discernable evidence.

F. Cell Viability

Cell viability on the rubber surface of the sampling chamber was tested by exposing cells to polymer for 0 (control), 1, 3, and 7 days. The percentages of cell numbers compared with the control ranged from 98% ± 0.8% (1 day) to 96% ± 0.9% (7 days). Thus, the polymer had no measurable effect on cell viability, which may be relevant to its expected effect on sampled microbiota.

G. Ex Vivo Experiments

Two meters of proximal jejunum were extracted from a freshly euthanized pig to test capsule sealing and activation. After visual inspection of their chambers to confirm they were empty, five capsules were inserted proximally into the intestine segment by hand, agitated by hand (with motion in all directions), and extracted distally. The sampling chamber contents were then examined subjectively (see Supplementary Video 2). The amount of digesta that entered into the capsules during this sealing test was insignificant.

An ex-vivo sampling test was also conducted using the intestine segment. Each of the same five capsules was then inserted proximally, moved to the mid-jejunum, and activated using a 2.5 cm cubic external magnet. Then, the capsule was distally removed and the capsule sampled content was observed (see Supplementary Video 2). In this sampling test, all five of the chambers contained significant amounts of digesta (Fig. 7f).

H. In Vivo Experiment

To test the capability to capture samples in a live animal, in vivo experiments were conducted, reviewed and approved by

the University of Guelph Animal Care Committee following Canadian Council on Animal Care guidelines [37]. Four capsules were fed with the aid of an injection tube in the pig's mouth to three pigs (age 7–8 weeks, body weight 15–20 kg) with a timing of 0 hr, 4 hr, 6 hr, and 8 hr. Thus 12 capsules in total were fed to the pigs. All capsules in the pigs were activated at the same time after 30.5 h by manual motion of the external magnet around the pig abdomen. The pigs were then euthanized, and the capsules were retrieved, immediately snapped frozen at –40°C, and stored at –90°C. The content of each capsule was then weighed and used for DNA analysis. Eleven of the twelve capsules successfully collected digesta in the range of 18 to 61 mg. The twelfth capsule did not appear to open and collected no digesta sample.

VI. Conclusion

A tetherless blindly activated capsule was developed for noninvasive microbiome sampling from all locations along the GI tract. The proposed capsule has three novel features. First, the outer shell is completely soft that permits noninvasive and safe passage without cross contamination through the GI tract. Second, the capsule is small and digestible, and can hold a large microbiome sample. Third, it can be remotely oriented by external magnetic actuation, which permits sample collection even when its location and orientation are not precisely known. As the internal magnets are strong, a novel composite was developed to reinforce the capsule, permitting it to tolerate the magnetic force generated between magnets and enhancing the strength of body and hinge. The capsule was tested and successfully actuated *ex vivo* and in an *in vivo* swine model. It successfully collected well-sealed samples. This simple sampling apparatus can contribute to the technological advancement required for breakthroughs in sequencing and microbial system and metabolite identification.

Acknowledgment

This work was supported by a New Ideas Fund grant from the University of Toronto Medicine by Design. We thank Dr. Elnaz Shokrollahi for her professional photos, Doug Wey for animal tests, Tomas Bernreiter for tensile tests, Ana Popovic for data extraction, and Mohammad H. Mohammadi for the viability test. There is no relationship between any author and the sources of financial support for this work.

References

[1] J. S. Biteen et al., "Tools for the microbiome: nano and beyond," *ACS Nano*, vol. 10, no. 1, pp. 6–37, Jan. 2016.

[2] J. M. Kinross, A. W. Darzi, and J. K. Nicholson, "Gut microbiome-host interactions in health and disease," *Genome Med.*, vol. 3, no. 3, p. 14, Mar. 2011.

[3] (2019) Impact of IBD in Canada report. Crohn's and Colitis Canada. [Online]. Available: https://crohnsandcolitis.ca/About-Us/Resources-Publications/Impact-of-IBD-Report

[4] G. Donaldson et al., "Gut biogeography of the bacterial microbiota," *Nat. Rev. Microbiol.*, vol. 14, no. 1, pp. 20–32, Jan. 2016.

[5] B. Wang et al., "The human microbiota in health and disease," *Engineering*, vol. 3, no. 1, pp. 71–82, 2017.

[6] J. C. Clemente et al., "The impact of the gut microbiota on human health: an integrative view," *Cell*, vol. 148, no. 6, pp. 1258–1270, Mar. 2012.

[7] G. Lv et al., "The gut microbiota, tumorigenesis, and liver diseases," *Engineering*, vol. 3, no. 1, pp. 110–114, 2017.

[8] Y. Wang et al., "Modulation of gut microbiota in pathological states," *Engineering*, vol. 3, no. 1, pp. 83–89, 2017.

[9] S. A. Fillon et al., "Novel device to sample the esophageal microbiome–the esophageal string test," *PLoS One*, vol. 7, no. 9, e42938, Sep. 2012.

[10] D. R. F. Elliott et al., "A non-endoscopic device to sample the oesophageal microbiota: a case-control study," *Lancet Gastroenterol. Hepatol.*, vol. 2, no. 1, pp. 32–42, Jan. 2017.

[11] S. M. Huse et al., "Comparison of brush and biopsy sampling methods of the ileal pouch for assessment of mucosa-associated microbiota of human subjects," *Microbiome*, vol. 2, no. 1, p. 5, Feb. 2014.

[12] K. Kerkhof et al., "Fluid Sampling Device," U.S. Patent Application 16/333,684, 2019.

[13] M. L. Jones et al., "Systems and methods for obtaining samples using ingestible device," U.S. Patent Application 15/680,400. 2018.

[14] J. Cui et al., "The study of a remote-controlled gastrointestinal drug delivery and sampling system," *Telemed. e-Health*, vol. 14, no. 7, pp. 715–719, Sep. 2008.

[15] F. Li et al., "Retention of the capsule endoscope: a single-center experience of 1000 capsule endoscopy procedures," *Gastrointest. Endosc.*, vol. 68, no. 1, pp. 174–180, Jul. 2008.

[16] M. Rezapour et al., "Retention associated with video capsule endoscopy: systematic review and meta-analysis," *Gastrointest. Endosc.*, vol. 85, no. 6, pp. 1157–1168.e2, 2017.

[17] E. Diller and M. Sitti, "Micro-scale mobile robotics," *Found. Trends Robot*, vol. 2, no. 3, pp. 143–259, Sep. 2013.

[18] E. Diller et al., "Assembly and disassembly of magnetic mobile micro-robots towards deterministic 2-D reconfigurable micro-systems," *Int. J. Rob. Res.*, vol. 30, no. 14, pp. 1667–1680, 2011.

[19] M. Sitti et al., "Biomedical applications of untethered mobile milli/microrobots," *Proc. IEEE*, vol. 103, no. 2, pp. 205–224, 2015.

[20] F. Carpi et al., "Magnetically controllable gastrointestinal steering of video capsules," *IEEE Trans. Biomed. Eng.*, vol. 58, no. 2, pp. 231–234, 2011.

[21] A. W. Mahoney and J. J. Abbott, "Managing magnetic force applied to a magnetic device by a rotating dipole field," *Appl. Phys. Lett.*, vol. 99, no. 13, p. 134103, 2011.

[22] H. Keller et al., "Method for navigation and control of a magnetically guided capsule endoscope in the human stomach," in *2012 4th IEEE RAS & EMBS International Conference on BioRob*, 2012, pp. 859–865.

[23] A. J. Petruska and J. J. Abbott, "An omnidirectional electromagnet for remote manipulation," in *2013 IEEE International Conference on Robotics and Automation*, 2013, pp. 822–827.

[24] F. Munoz et al., "A review of drug delivery systems for capsule endoscopy," *Adv. Drug Deliv. Rev.*, vol. 71, pp. 77–85, 2014.

[25] S. Yim and M. Sitti, "Design and rolling locomotion of a magnetically actuated soft capsule endoscope," *IEEE Trans. Robot.*, vol. 28, no. 1, pp. 183–194, 2012.

[26] W. Yu et al., "A smart capsule with GI-tract-location-specific payload release," *IEEE Trans. Biomed. Eng.*, vol. 62, no. 9, pp. 2289–2295, 2015.

[27] J. Flemming et al., "Small bowel capsule endoscopy," *Medicine*, vol. 97, no. 14, 2018

[28] S. H. Ku et al., "General functionalization route for cell adhesion on non-wetting surfaces," *Biomaterials*, vol. 31, no. 9, pp. 2535–2541, 2010.

[29] F. Carpi et al., "Controlled navigation of endoscopic capsules: concept and preliminary experimental investigations," *IEEE Trans. Biomed. Eng.*, vol. 54, no. 11, pp. 2028–2036, 2007.

[30] M. Sitti, *Mobile Microrobotics*. Cambridge: MIT Press, 2017.

[31] V. Paget, "Specific uptake and genotoxicity induced by polystyrene nanobeads with distinct surface chemistry on human lung epithelial cells and macrophages," *PloS one*, vol. 10, no. 4, p. 01232972015, 2015.

[32] E. P. Furlani, "Permanent magnet and electromechanical devices: materials, analysis, and applications," *Academic Press*, Sep. 2001.

[33] D. Brown. (Sep. 2017). Tracker. *Tracker*. [Online]. Available: https://physlets.org/tracker/

[34] D. K. Owens and R. C. Wendt, "Estimation of the surface free energy of polymers," *J. Appl. Polym. Sci.*, vol. 13, no. 8, pp. 1741–1747, Aug. 1969.

[35] J. Curtis and A. Colas "Medical applications of silicones," *Biomater. Sci.*, Academic Press, pp. 1106–1116, Jan. 2013.

[36] E. T. Hillman et al., "Microbial Ecology along the Gastrointestinal Tract," Microbes Environ. Vol. 32, no. 4, pp. 300–313, Dec. 2017.

[37] *The care and use of farm animals in research, teaching and testing* , Canadian Council on Animal, CCAC., Ottawa, ON, Canada, pp. 12–15, 2009.